

Article

Fabrication of Stretchable Copper Coated Carbon Nanotube Conductor for Non-Enzymatic Glucose Detection Electrode with Low Detection Limit and Selectivity

Dawei Jiang¹, Zhongsheng Liu², Kunkun Wu¹, Linlin Mou², Raquel Ovalle-Robles³, Kanzan Inoue³, Yu Zhang^{4,5}, Ningyi Yuan¹, Jianning Ding¹, Jianhua Qiu¹, Yi Huang² and Zunfeng Liu^{1,2,*}

¹ School of Materials Science and Engineering, Jiangsu Collaborative Innovation Center of Photovoltaic Science and Engineering, Changzhou University, Changzhou 213164, China; 18652856837@163.com (D.J.); wukunkun1030342792@163.com (K.W.); nyuyuan@cczu.edu.cn (N.Y.); dingjn@cczu.edu.cn (J.D.); jhqiu@cczu.edu.cn (J.Q.)

² State Key Laboratory of Medicinal Chemical Biology, Key Laboratory of Functional Polymer Materials, Ministry of Education, College of Pharmacy, Nankai University, Tianjin 300071, China; 13222539532@163.com (Z.L.); 13672133169@163.com (L.M.); yihuang@nankai.edu.cn (Y.H.)

³ Lintec of America, Nano-Science and Technology Center Richardson, Dallas, TX 75081, USA; raquel-ovalle@lintec-nstc.com (R.O.-R.); kz-inoue@lintec-nstc.com (K.I.)

⁴ Department of Building Engineering, Logistics University of PAPE, Tianjin 300309, China; zhangyu1983xinxin@163.com

⁵ College of Civil Engineering, Tongji University, Shanghai 200092, China

* Correspondence: liuzunfeng@nankai.edu.cn; Tel.: +86-131-148-88093

Received: 13 January 2018; Accepted: 19 March 2018; Published: 28 March 2018



Abstract: The increasing demand for wearable glucose sensing has stimulated growing interest in stretchable electrodes. The development of the electrode materials having large stretchability, low detection limit, and good selectivity is the key component for constructing high performance wearable glucose sensors. In this work, we presented fabrication of stretchable conductor based on the copper coated carbon nanotube sheath-core fiber, and its application as non-enzymatic electrode for glucose detection with high stretchability, low detection limit, and selectivity. The sheath-core fiber was fabricated by coating copper coated carbon nanotube on a pre-stretched rubber fiber core followed by release of pre-stretch, which had a hierarchically buckled structure. It showed a small resistance change as low as 27% as strain increasing from 0% to 500% strain, and a low resistance of $0.4 \Omega \cdot \text{cm}^{-1}$ at strain of 500%. This electrode showed linear glucose concentration detection in the range between 0.05 mM and 5 mM and good selectivity against sucrose, lactic acid, uric acid, acrylic acid in phosphate buffer saline solution, and showed stable signal in high salt concentration. The limit of detection (LOD) was 0.05 mM, for the range of 0.05–5 mM, the sensitivity is $46 \text{ mA} \cdot \text{M}^{-1}$. This electrode can withstand large strain of up to 60% with negligible influence on its performance.

Keywords: carbon nanotube; elastic conductor; buckle structure; non-enzymatic glucose detection

1. Introduction

Stretchable conductors having stable resistance and high conductivity are key components for wearable electronics [1–6]. An efficient way to fabricate stretchable conductors is to use a conducting layer with buckled structure. Such a structure is prepared by coating conductive layer over a pre-stretched elastomeric polymer substrates followed by relax of the prestrain [7–12]. During stretching the buckled

surface layer fattens without broken and therefore kept resistance constant. The generally used material for the surface conducting layer is metal or semiconductor film, carbon nanotubes, graphene, or conducting polymer fibers. One of the limitations of using metal film is that the buckled metal film based stretchable conductor can only withstand very limited strain range (e.g., 10% for gold film coated on PDMS) [13]. By using buckled silver nanowires or carbon nanotubes as the conducting layer, the resulting stretchable conductors can have an available strain range less than 100% [14,15]. Recently, forest drawn super aligned carbon nanotube sheets (SACNSs) have been used to fabricate the buckled conducting surface layer of the stretchable conductors and the available strain can be improved to 400% [16–18]. In our recent work, we have prepared hierarchically buckled structure using SACNS and realized a resistance change less than 5% for over 1000% strain, pushing the stretchability to a record value with obtaining stable resistance [19,20]. As the conductivity of carbon is relatively low, one limitation of such stretchable conductors is that they are suitable for applications that require low conductivity. For example, for constructing wearable glucose sensors that can be used for real time monitoring the glucose concentration, a stretchable electrode with high conductivity and stable resistance is required.

Wearable glucose sensors can measure the glucose concentration in body fluid such as sweat, saliva, and tears [21–23]. The normal blood sugar level is in the range of about 4.4 to 6.1 mM [24], and the glucose concentration in sweat was about 1% of that in blood [25]. This means that a detection limit of glucose around 0.05 mM is required for sweat glucose detection. This detection limit of glucose concentration in sweat is much lower than that in blood. Moreover, to provide real time and on-body glucose monitoring, flexibility and stretchability of the electrode is required. Because there is considerable deformation in the skin during people's movement (e.g., 60% in elbow), high stretchability is preferred [26]. Furthermore, the amperometric response of the electrode was generally interfered by endogenous electro-active chemicals, including sucrose, acrylic acid (AA), lactose, and uric acid (UA). Although these chemicals only presented at much lower concentration than glucose in the body fluids, they may also cause interference for glucose sensing. Therefore, fabrication of the glucose sensing electrode showing high stretchability, a low detection limit, and selectivity is required for high performance non-invasive on body glucose monitoring.

There are two types of electrodes for glucose sensing: enzymatic and non-enzymatic. Enzymatic electrodes have been proven successful in detecting glucose concentrations [27–31]. However, they are limited by the instability of the enzyme, which is easily influenced by pH, temperature, humidity, and oxygen [32]. The non-enzymatic electrodes for glucose detection use metal, metal oxide, carbon nanomaterials, and the combinations of the above two or more species as active materials. During glucose detection, the glucose molecules bind to the electrode and change its electrochemical environment, which serves as an electrochemical catalyst for oxidation of the glucose molecules [5,33]. Compared to the enzymatic counterparts, the non-enzymatic electrodes show much higher stability [34–41]. Recently, there has been rapid development of flexible and stretchable non-enzymatic electrodes, including single metal or metal oxide (Au, Ag [42,43], Pt, Ni [44], NiO [41,45,46], Cu, CuO [47]), bimetallic components (Ag/Cu [48], Pd/Pt [49]), and carbon nanomaterials functionalized with metals [27], as listed in Table 1. Although these recently-developed non-enzymatic electrodes show properties including flexibility or stretchability, low detection limit, and anti-interference, it is still a challenge to prepare a non-enzymatic electrode with the combination of high strain, low detection limit, and selectivity.

Table 1. Comparison of the non-enzymatic stretchable and flexible glucose sensing electrodes with selectivity against interferents.

Electrode	V _{App.} ¹ (V)	LOD ² (μM)	Strain (%)	Selectivity Test	Reference
Graphene/CNT ³ /Ionic Liquid	+0.2	100	Flexible	DA ⁴ /AA ⁵ /UA ⁶ /NaCl	[36]
3D CuO Nanowire Arrays	+0.35	20	Flexible	AA/Lactose/Maltose	[45]
PtAu-MnO ₂ /Graphene Paper	0	20	Flexible	DA/AA/UA	[46]
Ni/VCNTs ⁷ /Graphene	+0.5	30	Flexible	AA/GA ⁸ /XY ⁹ /UA	[47]
NiO QDs ¹⁰ -ZnO NRs ¹¹ / Polyimide	n/a	26	Flexible	DA/AA/UA/cholesterol	[48]
Au Nanoparticles/Polyaniline/ Carbon Cloth	0	12.6	Flexible	AA/UA/AMP ¹² / D-galactose/fructose	[49]
Cu Nanoparticles/RGO ¹³	+0.6	1000	Flexible	AA/UA/DA	[50]
Pt/CNTS ¹⁴ /Rubber	+0.3	660	45%	n/a	[51]
Pt-Graphite	+0.3	4800	75%	AA/UA/DP ¹⁵ /EPI ¹⁶	[52]
Cu/CNTS/Rubber	+0.35	50	60%	AA/Sucrose/Lactose/UA/NaCl	This work

¹ V_{app.}: Applied Potential; ² LOD: Limit of Detection; ³ CNTS: Carbon Nanotube; ⁴ DA: Dopamine; ⁵ AA: Ascorbic Acid; ⁶ UA: Uric Acid; ⁷ VCNTs: Vertically Aligned Carbon Nanotubes; ⁸ GA: Galactose; ⁹ XY: Xylose; ¹⁰ NiO QDs: Nickel Oxide Quantum Dots; ¹¹ ZnO NRs: Zinc Oxide Nanorods; ¹² AMP: Adenosine Monophosphate; ¹³ RGO: Reduced Graphene Oxide; ¹⁴ CNTS: Carbon Nanotube Sheets; ¹⁵ DP: Docking Protein; ¹⁶ EPI: Epirubicin.

In our recent work, by using buckled Pt-coated CNTS based sheath-core conductors, we showed glucose detection under large deformation up to 45% with stable performance. This stretchable electrode showed linear relationship of current with glucose concentration between 0.67 mM and 10.5 mM in phosphate buffer saline (PBS) solution [26]. Here, our strategy is to further modify the above CNTS based stretchable electrode to obtain lower detection limit and introduce selectivity for glucose detection.

There have been several important studies to decrease the detection limit and minimize the interference in glucose sensing caused by the electroactive species in blood fluid [25,53–55]. One important strategy is to use Cu and CuO nanoparticles functionalized carbon nanomaterials such as carbon nanotubes, graphene, and carbon black [26,56–60]. This is possibly because of the combination of high catalytic activity of Cu/CuO nanoparticles for glucose oxidation and high electrochemical activity and conductivity of the carbon nanomaterials. Up to now, there has not been a report about fabrication of highly stretchable copper coated carbon nanomaterials used for glucose detection.

Based on these considerations, in this paper we fabricated highly stretchable conductors based on copper coated carbon nanotube sheath-core fibers, and characterized their applications in non-enzymatic glucose sensing electrode with high stretchability, low detection limit, and selectivity. The sheath-core conductor was fabricated by coating copper coated carbon nanotube sheet on a pre-stretched rubber fiber core followed by release of pre-stretch, which showed a hierarchically buckled structure. It showed a small resistance change as low as 27% as strain increasing from 0% to 500% strain, and a low resistance of 0.4 Ω cm⁻¹ at 500% strain. In a proof of principle study, this electrode showed linear glucose concentration detection in the range between 0.05 mM and 5 mM and good selectivity against sucrose, lactose, uric acid, and acrylic acid in phosphate buffer saline solution, and showed stable signal in high salt concentration. This electrode can withstand large strain of up to 60% with negligible influence on its performance. Our results push the sheath-core fiber technology for precise measurements of glucose concentration to a much closer step to real applications.

2. Materials and Methods

The CNTS used in this work was drawn from spinnable carbon nanotube forest (~6 walls, ~10 nm in diameter, and ~350 μm high) grown by chemical vapor deposition (CVD) method. The rubber contains a mixture of styrene-(ethylene-butylene)-styrene (SEBS, G-1651H, Kraton, Houston, TX, USA) and liquid wax (Marcol 82, ExxonMobil, Irving, TX, USA) with a weight ratio of 1/5.

Fabrication of copper coated CNTS (Cu_t-CNTS) is as follows, where *t* means the thickness of the copper layer. The Cu_t-CNTS was prepared by coating a copper thin layer on the CNTS via magnetron sputter deposition. The samples with different copper thickness were prepared using a Cu target with

8-cm diameter and purity of 99.99%. The holder containing CNTS was rotated during deposition of Cu in order to obtain uniform Cu layer on the CNTS. The distance between the Cu target and the CNTS was 15 cm. A copper plate cooled by water was used to mount the cathode. A base pressure of 1.8×10^{-3} Pa in the chamber was realized before deposition of Cu. High purity argon was used as the working gas and the pressure during Cu deposition was 0.6 Pa. The copper thickness was determined using the Alpha-Step 500 surface profiler for the metal film deposited on the glass slide. The deposition rate of copper was calculated to be $1.4 \text{ nm} \cdot \text{min}^{-1}$, by dividing the film thickness with time.

The fabrication of copper coated CNTS based stretchable conductive fibers ($\text{Cu}_t\text{-CNTS@fibers}$) was based on a pre-stretch/release method. Briefly, we stretched the rubber fiber of 2 mm in diameter to a fabrication strain (800% if not specified). Then a thin layer of rubber about $3 \mu\text{m}$ was coated on the pre-stretched rubber fiber in order to improve the adhesion of $\text{Cu}_t\text{-CNTS}$ on rubber. Then $\text{Cu}_t\text{-CNTS}$ supported on a frame was attached on the surface of the pre-stretched rubber fiber coated with a rubber thin layer. An important thing was that the $\text{Cu}_t\text{-CNTS}$ was aligned with the stretching direction of rubber fiber. After rolling $\text{Cu}_t\text{-CNTS}$ layers, the $\text{Cu}_t\text{-CNTS}$ was densified onto the rubber surface by dropping ethanol (98%). Then pre-stretched rubber fiber was slowly relaxed to produce the buckled $(\text{Cu}_t\text{-CNTS})_m\text{@fibers}$ after ethanol evaporation.

Characterization of $\text{Cu}_t\text{-CNTS}$ and $(\text{Cu}_t\text{-CNTS})_m\text{@fibers}$: The electrical resistance was measured by using a two-probe method via a Keithley SourceMeter modeled 2400 in N_2 atmosphere. The scanning electron microscope (SEM) micrographs were taken on a Nova NanoSEM450 field emission SEM.

Glucose concentration measurements using the $(\text{Cu}_t\text{-CNTS})_m\text{@fiber}$ electrode: A three-electrode system was used to measure the amperometric response of glucose concentration using $(\text{Cu}_t\text{-CNTS})_m\text{@fibers}$, including a $(\text{Cu}_t\text{-CNTS})_m\text{@fiber}$ as the working electrode, a Pt wire as the counter electrode, and an Ag/AgCl (KCl-saturated) electrode as the reference electrode, respectively. For all experiments, PBS solution (NaCl: 137 mM, KCl: 2.7 mM, Na_2HPO_4 : 10 mM, KH_2PO_4 : 1.8 mM, pH 7.4) and the analyte solutions were freshly prepared. Cyclic voltammograms (CV) of the $(\text{Cu}_{13\text{nm}}\text{-CNTS})_3\text{@fiber}$ electrode and the $\text{CNTS}_3\text{@fiber}$ electrode in PBS solution were obtained at different strain, using a scan rate of 100 mV s^{-1} unless otherwise mentioned. The CV curves were obtained at different applied potentials in PBS solution by dropwise addition of glucose and other interferents under magnetically stirred conditions. By adding one drop of glucose, the glucose concentration increased by 0.05 mM in the detection solution, and the applied potentials were +0.25 V, +0.35 V, +0.5 V. Amperometric current–time data were collected under magnetically stirring at a constant applied potential. Repeatability was characterized by measuring the relative amperometric response of the electrode to addition of 1 mM glucose into PBS solution over a period of 72 h with interval of 12 h. The electrode was taken out, washed thoroughly with H_2O , and put in the ambient condition between the two measurements. After the current curve reached a steady state, the solutions of analyte and interferents were injected. Here, nine samples (three samples from three separate batches) were used. Electrochemical measurements were performed on a CH Instruments (CHI) 660C electrochemical analyzer, and the data were analyzed using the CHI software.

3. Results and Discussion

3.1. Electrical Properties of $(\text{Cu}_t\text{-CNTS})_m\text{@fibers}$

The CNTS were drawn from a CNT forest which was grown by using a CVD method, and the carbon nanotube bundles were aligned in the drawing direction of the CNTS. The diameter of the individual nanotubes was about 10 nm, and the CNTS was a continuous sheet that was formed by interconnection of the carbon nanotube bundles. The thickness of the as-drawn CNTS sheet was $18 \mu\text{m}$ [61]. The CNTS showed a highly porous and loose aerogel structure, which allowed the magnetron sputtered species to easily pass through the nanotube sheets and disperse over the CNT bundles, as shown in Figure 1.

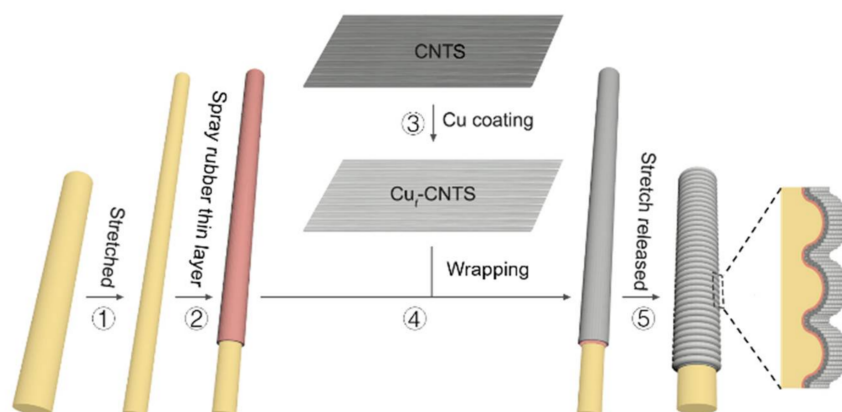


Figure 1. Schematic demonstration of fabrication of $(\text{Cu}_t\text{-CNTS})_m@$ fibers. The numbers indicate the fabrication steps.

Magnetron sputter deposition was widely used to deposit thin metal films for diverse applications because of its high rate, ease of scaling, and high quality of the deposited film [62]. Here, the copper was deposited on the CNTS using magnetron sputter deposition to improve the conductivity and electro-catalytic activity. The sheet resistance for an as-produced single CNTS was $\sim 1000 \Omega$ per square (equal to 1 S mm^{-1}) in the drawing direction, which was relatively high for applications in interconnects for electric circuits and sensing electrodes. After copper deposition, we tested the resistance in N_2 atmosphere. The sheet conductance increased from 11.2 S mm^{-1} to 32.3 S mm^{-1} with the deposition time of copper increasing from 40 s to 160 s, corresponding to an average conductance increasing rate of $0.18 \text{ S mm}^{-1} \text{ s}^{-1}$. With further increasing the deposition time from 160 s to 700 s, the sheet conductance increased dramatically from 32.3 S mm^{-1} to 9577 S mm^{-1} , corresponding to an average conductance increasing rate of $17.7 \text{ S mm}^{-1} \text{ s}^{-1}$ (Figure 2).

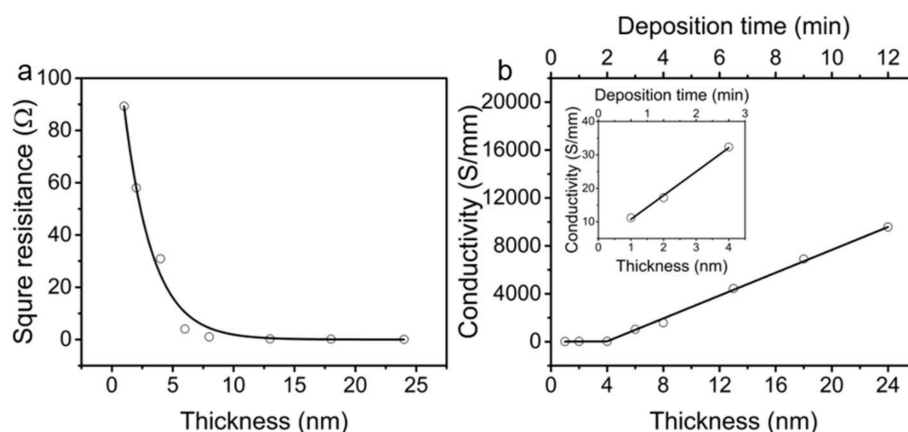


Figure 2. (a) The square resistance of the $\text{Cu}_t\text{-CNTS}$ as a function of Cu thickness. (b) The conductivity of the $\text{Cu}_t\text{-CNTS}$ as a function of deposition time and thickness of Cu. The inset showed conductance of $\text{Cu}_t\text{-CNTS}$ as a function of deposition time and thickness of Cu for deposition time shorter than three minutes.

Figure 3 showed the SEM images of the surface for $\text{Cu}_t\text{-CNTS}$ samples with different deposition time. For deposition time from 60 s to 240 s, discrete Cu nanoparticles were observed on the carbon nanotube surface. For these samples, although the conductance increased with increasing Cu deposition time, the Cu nanoparticles with an average thickness of 8 nm did not form a continuous pathway (Figure 3b). Therefore, the conductance increased relatively slow with increasing the deposition time. With further increasing the

deposition time to 400 s (thickness of Cu layer is about 13 nm), uniform surface was observed (Figure 3c). The copper nanoparticles contacted with one another and formed continuous pathway, and therefore the conductance should be dominated by the copper sheath coated over the carbon nanotube bundles, which should be responsible for the rapid increase in the conductance with increase of the thickness of Cu layer. The thickness of Cu coating was obtained by measuring the thickness of the deposited film on a glass slide. For the convenience of nomenclature, the average thickness of the $\text{Cu}_t\text{-CNTS}$ samples with discrete Cu nanoparticles was also normalized to those having continuous Cu layer by counting the deposition time, as shown in Figure 3. It is worth noticing that the actual thickness of the Cu layer might be smaller than that of the film coated on the glass slide because the bundles of the CNT were not continuous so that some Cu atoms may pass through the gaps between the CNT bundles. From the SEM image of the surface of $\text{Cu}_{24\text{nm}}\text{-CNTS}$ (Figure 3d), we can clearly see that a continuous Cu layer was coated on the CNT bundle. The remarkable conductance and highly alignment architecture of the $\text{Cu}_t\text{-CNTS}$ allowed the fabrication of superelastic sheath–core conductors [55].

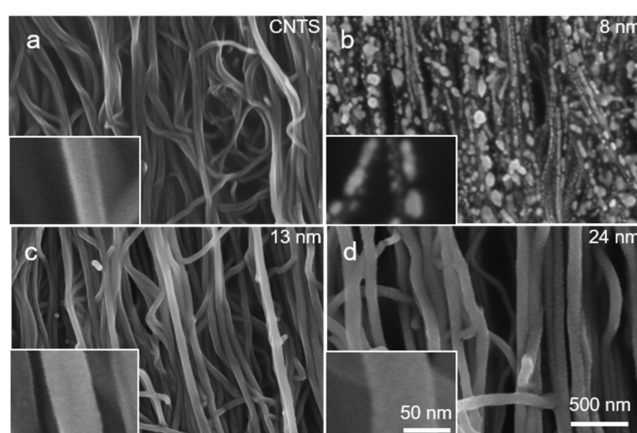


Figure 3. (a–d) The SEM images of the $\text{Cu}_t\text{-CNTS}$ with different thickness of copper.

We fabricated the sheath-core $(\text{Cu}_t\text{-CNTS})_m\text{@fibers}$ by using a similar method to our previous work for CNTS based sheath-core fiber [26,55,63,64], except that a very thin layer of rubber was coated over the pre-stretched rubber fiber in order to improve the adhesion of the $\text{Cu}_t\text{-CNTS}$ layer on the rubber fiber core. Briefly, we stretched a rubber fiber to the fabrication strain, and then sprayed with a thin layer of rubber (3 μm) over the rubber fiber core. We then coated layers of $\text{Cu}_t\text{-CNTS}$ on the pre-stretched rubber fiber. It should be noted that the orientation direction of the $\text{Cu}_t\text{-CNTS}$ was the same as the stretch direction of the rubber fiber. Ethanol was used to densify the porous $\text{Cu}_t\text{-CNTS}$ on the rubber fiber, and then we released the applied strain of the rubber fiber, as shown in Figure 1. The fiber diameter was typically 2 mm, and the fabrication strain was typically 800% if not specified.

Before characterization, the $\text{Cu}_t\text{-CNTS}$ sheath core fibers were trained for five cycles by repeatedly stretching the fiber to the fabrication strain and fully relaxing. We choose the fabrication strain of the $(\text{Cu}_t\text{-CNTS})_m\text{@fibers}$ as the maximum length because irreversible plastic deformation of the $\text{Cu}_t\text{-CNTS}$ would occur if when the $(\text{Cu}_t\text{-CNTS})_m\text{@fibers}$ are beyond the fabrication strain. Figure 4a,b showed the SEM images of the $(\text{Cu}_{13\text{nm}}\text{-CNTS})_3\text{@fiber}$, it can be seen that hierarchical buckling in the fiber length direction and necking in the circumferential direction occurred for the $\text{Cu}_{13\text{nm}}\text{-CNTS}$ conducting layer. The formation of buckling structure in the length direction and necking in the circumferential direction is because the rubber material is non-compressive (the Poisson's ratio of rubber is about 0.5). During the relaxation of the pre-stretched rubber fiber, the fiber length decreased by L times and the fiber diameter increased by $L^{-1/2}$ times accordingly. This length decrease caused buckle formation and the diameter increase caused stretch of the copper coated carbon nanotube sheath and then induced necking [65]. This two orders of hierarchically buckled structure of $(\text{Cu}_{13\text{nm}}\text{-CNTS})_3\text{@fiber}$ was different from the buckled structures of the $\text{CNTS}_m\text{@fibers}$, where one order of buckled structure

was observed if the number of CNTS layer was smaller than five [55]. Because a rubber thin layer was applied for adhesion before deposition of the $\text{Cu}_t\text{-CNTS}$ conducting layer during fabrication of $\text{CNTS}_m\text{@fibers}$, the two orders of hierarchical buckling structure of the $(\text{Cu}_{13\text{nm}}\text{-CNTS})_3\text{@fiber}$ may be a consequence of the buckling of the sprayed rubber adhesion layer superimposed with the buckling of CNTS layer during relaxation of the pre-strain of rubber fiber core [26]. The final $(\text{Cu}_{13\text{nm}}\text{-CNTS})_3\text{@fiber}$ showed smaller available strain range than the fabrication strain because of the mechanical confinement of the buckled $\text{Cu}_t\text{-CNTS}$ sheath layer. The available elastic strain range of the $(\text{Cu}_{13\text{nm}}\text{-CNTS})_3\text{@fiber}$ prepared in this paper could be up to 600%. CNT bundles coated with copper layer generated a metal-carbon hybrid conducting material with structural anisotropy. Because of the flexibility of the CNTS skeleton, the hybrid material should possess more flexibility compared to the metal thin film. Furthermore, the copper coated CNT bundles are continuous in stretch/release direction of the rubber fiber and discontinuous in the circumferential direction of the $(\text{Cu}_t\text{-CNTS})_m\text{@fibers}$. Therefore, it can accommodate circumferential expansion during large strain relaxation (up to 600% in our case) of the rubber fiber core. This is advantageous compared to the thin metal film based stretchable conductors, which can only withstand a limited strain of up to 22% for obtaining stable resistance and cracks would occur perpendicular to the stretch–release direction [66,67].

Increasing the copper thickness in the $\text{Cu}_t\text{-CNTS}$ hybrid layer resulted in decrease of resistance of the $(\text{Cu}_t\text{-CNTS})_m\text{@fibers}$. Figure 4c showed the results of length normalized resistance ($R(\epsilon)/L_\epsilon$) as a function of tensile strain (ϵ) of the $(\text{Cu}_t\text{-CNTS})_3\text{@fibers}$ having different Cu thickness (t), where $R(\epsilon)$ and $L(\epsilon)$ were the resistance and length at strain (ϵ) of the $(\text{Cu}_t\text{-CNTS})_m\text{@fibers}$. For the $(\text{Cu}_t\text{-CNTS})_3\text{@fibers}$ at 0% strain, $R(0)/L_0$ decreased from $19 \Omega\cdot\text{cm}^{-1}$ to $1.4 \Omega\cdot\text{cm}^{-1}$ as t increased from 4 nm to 24 nm. For the $(\text{Cu}_t\text{-CNTS})_3\text{@fibers}$ in the stretched state, $R(500\%)/L_{500\%}$ decreased from $4 \Omega\cdot\text{cm}^{-1}$ to $0.4 \Omega\cdot\text{cm}^{-1}$ as t increased from 4 nm to 24 nm, as shown in Figure 4c. $R(\epsilon)/L_\epsilon$ of the $(\text{Cu}_t\text{-CNTS})_3\text{@fibers}$ decreased monotonically with increase of strain (ϵ). For example, $R(\epsilon)/L_\epsilon$ of $(\text{Cu}_{4\text{nm}}\text{-CNTS})_3\text{@fiber}$ decreased from $19 \Omega\cdot\text{cm}^{-1}$ to $3 \Omega\cdot\text{cm}^{-1}$ as strain increased from 0% to 700%; $R(\epsilon)/L_\epsilon$ of $(\text{Cu}_{24\text{nm}}\text{-CNTS})_3\text{@fiber}$ decreased from $1.4 \Omega\cdot\text{cm}^{-1}$ to $0.4 \Omega\cdot\text{cm}^{-1}$ as strain increased from 0% to 500%.

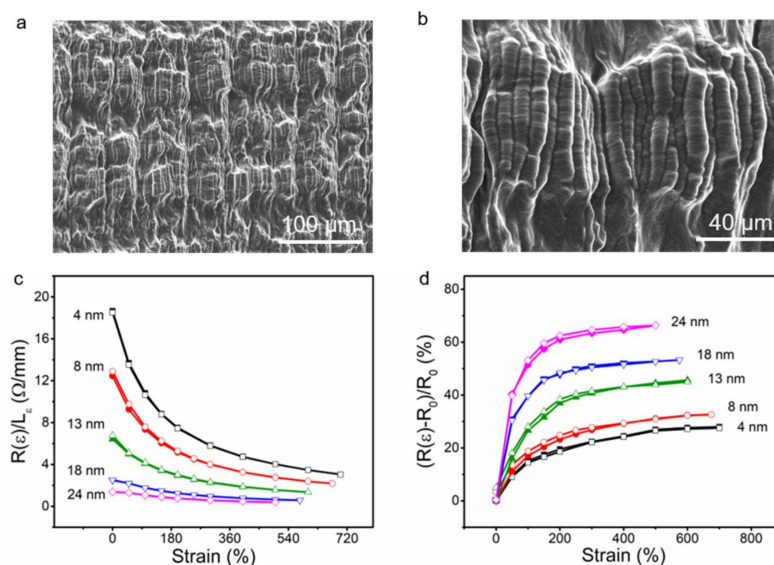


Figure 4. Low- (a) and high- (b) magnification SEM images of the $(\text{Cu}_{13\text{nm}}\text{-CNTS})_3\text{@fiber}$ at 0% strain. The circumferential direction is vertical and the length direction is horizontal. The resistance normalized to length (c) and percent resistance change (d) for $(\text{Cu}_t\text{-CNTS})_3\text{@fibers}$ as a function of applied strain with different thickness of copper layer. The solid symbols represented strain increase and the open symbols represented subsequent strain release. The fabrication strain was 800% and the fiber diameter was 2 mm for (a–d).

Figure 4d showed the percent resistance change $((R(\varepsilon)-R_0)/R_0)$ of the $(\text{Cu}_t\text{-CNTS})_3$ @fibers as a function of copper thickness (t), where R_0 is the resistance at 0% strain. It can be seen that the $(R(\varepsilon)-R_0)/R_0$ values of $(\text{Cu}_t\text{-CNTS})_3$ @fibers were 27, 31, 44, 53, and 66% for $t = 4, 8, 13, 18,$ and 24 nm, respectively, as strain increased from 0% to 500%. This indicated that the resistance of the $(\text{Cu}_t\text{-CNTS})_m$ @fibers decreased with increasing the thickness of the copper layer on the CNTS, and the resistance got less stable with strain increase. This is possibly because the flexibility of the $\text{Cu}_t\text{-CNTS}$ layer decreased with increase of the copper layer.

3.2. Stretchable Non-Enzymatic Electrode for Glucose Sensing Based on the $(\text{Cu}_t\text{-CNTS})_m$ @fibers

We then characterized the $(\text{Cu}_t\text{-CNTS})_m$ @fibers for used in non-enzymatic glucose detection. We constructed a three-electrode system including a working electrode using $(\text{Cu}_{13\text{nm}}\text{-CNTS})_3$ @fiber, a reference electrode using Ag/AgCl electrode, and a counter electrode using a platinum wire. Figure 5a,b showed CV of $(\text{Cu}_{13\text{nm}}\text{-CNTS})_3$ @fiber electrode in PBS solution at 0% strain with a scan rate of 100 mV s^{-1} , using CNTS_3 @fiber electrode as the control.

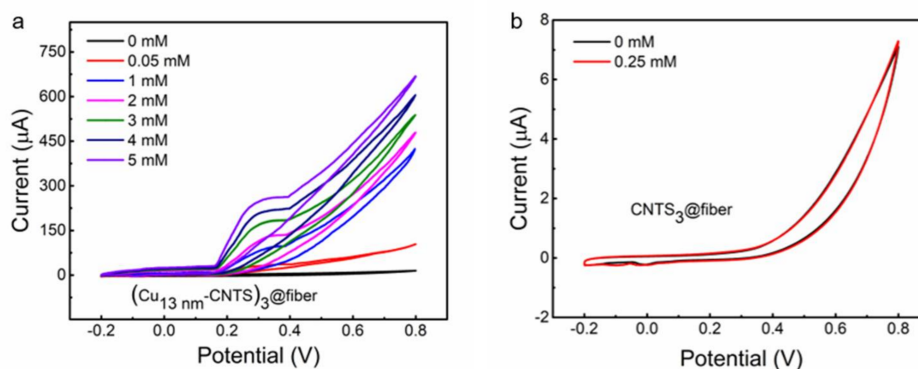


Figure 5. (a,b) Cyclic voltammograms of the $(\text{Cu}_{13\text{nm}}\text{-CNTS})_3$ @fiber electrode at different glucose concentrations (0, 0.05, 1, 2, 3, 4, and 5 mM) (a) and the CNTS_3 @fiber electrode (b) in PBS solution at 0% strain and 100 mV s^{-1} .

There were no substantial peaks observed for the CV of both $(\text{Cu}_{13\text{nm}}\text{-CNTS})_3$ @fiber and CNTS_3 @fiber without glucose addition, except for the tail-shaped peak occurred at $+0.65 \text{ V}$, which corresponded to the electrolysis of H_2O molecules, as shown in Figure 5a,b, respectively. Figure 5a showed that by adding different concentrations of glucose, the $(\text{Cu}_{13\text{nm}}\text{-CNTS})_3$ @fiber showed peaks of current appearing at $+0.35 \text{ V}$ and $+0.65 \text{ V}$ versus the Ag/AgCl electrode. The shoulder peak occurred at $+0.35 \text{ V}$ was ascribed to the glucose oxidation on copper. This indicated high catalytic capacity of copper coated CNTS for glucose oxidation to gluconic acid. In comparison, no new peaks were observed by the addition of glucose on the CNTS_3 @fiber electrode system as shown in Figure 5b, indicating that the pure CNTS can hardly be used for glucose sensing at the same electrochemical conditions.

It was reported that the amperometric signal of an electrochemical electrode was highly dependent on the applied potential. Below we studied the influence of applied potential on the amperometric signals of our $(\text{Cu}_{13\text{nm}}\text{-CNTS})_3$ @fiber electrode. These experiments were carried out on $(\text{Cu}_{13\text{nm}}\text{-CNTS})_3$ @fiber electrode at 0% strain, by dropwise addition of glucose into PBS solution at interval of 50 s by applying potential from $+0.25 \text{ V}$ to $+0.50 \text{ V}$. The dropwise addition of glucose resulted in step-wise increase of glucose concentration.

Figure 6a showed the current was very low at an applied potential of $+0.25 \text{ V}$, and the current of $(\text{Cu}_{13\text{nm}}\text{-CNTS})_3$ @fiber electrode increased remarkably at the applied potentials of $+0.35 \text{ V}$ and $+0.5 \text{ V}$. Figure 6b showed the dependence of current on the $(\text{Cu}_{13\text{nm}}\text{-CNTS})_3$ @fiber electrode on glucose concentration from 0.05 mM to 2.5 mM at different applied potentials, with 0.05 mM and 0.5 mM for low and high glucose concentration regions. The calibration curve of the current showed linear

response with increase of the glucose concentration at the investigated potentials from nine samples (three samples from three separate batches). It is noticeable that the application of potential of +0.35 V vs. Ag/AgCl on the working electrode was close to the voltage corresponding to glucose oxidation, where the current peak was observed from the CV curve of the $(\text{Cu}_{13\text{nm}}\text{-CNTS})_3\text{@fiber}$. At the working potential of +0.35 V, the sensitivity of the $(\text{Cu}_{13\text{nm}}\text{-CNTS})_3\text{@fiber}$ electrode at 0% strain was calculated to be $\sim 46 \text{ mA}\cdot\text{M}^{-1}$ for the investigated glucose concentration range of 0.05–5 mM, by dividing the detected current change with glucose concentration change. The limit of detection (LOD) is 0.05 mM. By considering the glucose oxidation peak around +0.35 V, as well as the reasonable electrochemical current and linear relationship were obtained at this potential, +0.35 V was applied as the working potential in the following investigations for stretchability, selectivity, and stability tests.

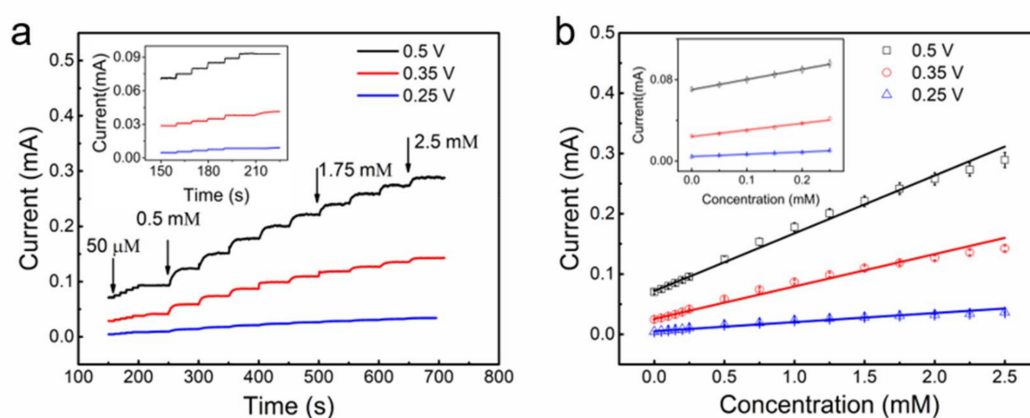


Figure 6. (a) Current as a function of time of the $(\text{Cu}_{13\text{nm}}\text{-CNTS})_3\text{@fiber}$ electrode at different applied potentials in PBS solution by dropwise addition of glucose. (b) The calibration curve of the current as a function of concentration of the $(\text{Cu}_{13\text{nm}}\text{-CNTS})_3\text{@fiber}$ electrode at different applied potential, nine samples (three samples from three separate batches) are used here to get the average values. For (a,b), by adding one drop of glucose, the glucose concentration increased by 0.05 mM for the low concentration range and 0.5 mM for the high concentration range, and the applied potentials were +0.25, +0.35, and +0.5 V. Insets: current as a function of time for low concentration range of glucose for both (a,b).

Figure 7a showed current during stepwise drop addition of glucose for the $(\text{Cu}_{13\text{nm}}\text{-CNTS})_3\text{@fiber}$ electrode at strain of 0, 15, 30, 45, and 60%, respectively. It can be seen that the detected current almost unchanged for the investigated glucose concentration range from 0.05 mM to 0.5 mM for the investigated strain level. This indicated that our $(\text{Cu}_t\text{-CNTS})_m\text{@fiber}$ electrode showed good stability for non-enzymatic glucose detection under large deformations.

To quantitatively investigate the stability of glucose detection during deformation, we calculated the quality factor for glucose sensing (Q_{gs}) of the $(\text{Cu}_{13\text{nm}}\text{-CNTS})_3\text{@fiber}$ electrode for the strain range from 0% to 60%. The Q_{gs} was calculated by the Equation (1)

$$Q_{\text{gs}} = ((I(\varepsilon) - I_0)/I_0)/(\varepsilon - 0\%) \quad (1)$$

where $I(\varepsilon)$ and I_0 are the current at strain of ε and 0%, respectively. The calculated value of Q_{gs} of the $(\text{Cu}_{13\text{nm}}\text{-CNTS})_3\text{@fiber}$ electrode was about 30 for the strain range from 0% to 60%, which was higher than our previously investigated glucose sensing system of platinum coated CNTS based stretchable electrode ($Q_{\text{gs}} = 22$ for strain range from 0% to 45%). This high stability during large deformation for glucose sensing of the $(\text{Cu}_t\text{-CNTS})_m\text{@fiber}$ electrode made it a promising candidate for constructing wearable sensors for non-enzymatic glucose monitoring during extreme on-body deformation.

We then characterized the selectivity of our stretchable $(\text{Cu}_t\text{-CNTS})_m\text{@fiber}$ electrode against interferences—including sucrose, AA, lactose, and UA—as well as in high salt concentration. These chemicals were generally present in human physiological fluids and blood serum accompanying with glucose. Although the glucose concentration in human blood in normal physiological conditions was much higher (about 30 times) than that of the sucrose, AA, lactose, and UA [57], we used a higher level of interferent species to test the selectivity of the $(\text{Cu}_t\text{-CNTS})_m\text{@fiber}$ electrode. We successively added glucose (0.05 mM, the final concentration, and the same for the following chemicals) and sucrose (0.008 mM), AA (0.008 mM), lactose (0.008 mM), NaCl (150 mM), and UA (0.008 mM) into PBS solution by dropwise addition of glucose and the relevant interfering species at an applied potential of +0.35 V, and the results were shown in Figure 7b. With addition of glucose, we can clearly see the amperometric response, while by adding sucrose, AA, lactose, and UA, the $(\text{Cu}_{13\text{nm}}\text{-CNTS})_3\text{@fiber}$ electrode did not show any significant current increase. These results indicated that $(\text{Cu}_{13\text{nm}}\text{-CNTS})_3\text{@fiber}$ electrode could be used as a highly selective electrode for glucose detection. Furthermore, the $(\text{Cu}_{13\text{nm}}\text{-CNTS})_3\text{@fiber}$ electrode also showed negligible change of the response by addition of high concentration of NaCl. We then studied the stability and long-term repeatability of the $(\text{Cu}_{13\text{nm}}\text{-CNTS})_3\text{@fiber}$ electrode from nine samples (three samples from three separate batches). Figure 8a showed that there was negligible signal loss in current over 1000 s of running time, indicating good stability of the electrode. The inset in Figure 8a showed the repeated measurements of the relative amperometric response of the electrode to addition of 1 mM glucose into PBS solution over a period of 72 h with interval of 12 h. The final relative amperometric response was 94.5% of the initial value after 72 h, indicating good repeatability and long-term stability of the electrode. Compared to the stretchable glucose sensing electrodes [28,29,56], our non-enzymatic electrode based on $(\text{Cu}_t\text{-CNTS})_m\text{@fibers}$ showed simultaneous combination of high stretchability (60%), high sensitivity ($46 \text{ mA}\cdot\text{M}^{-1}$), low limit of detection (0.05 mM), high selectivity, and the nature of non-enzymatic detection. Figure 8b showed the consecutive measurements of the $(\text{Cu}_{13\text{nm}}\text{-CNTS})_3\text{@fiber}$ electrode in glucose solution from low concentration to high concentration, and then back to low concentrations, indicating the good reversibility of the electrode.

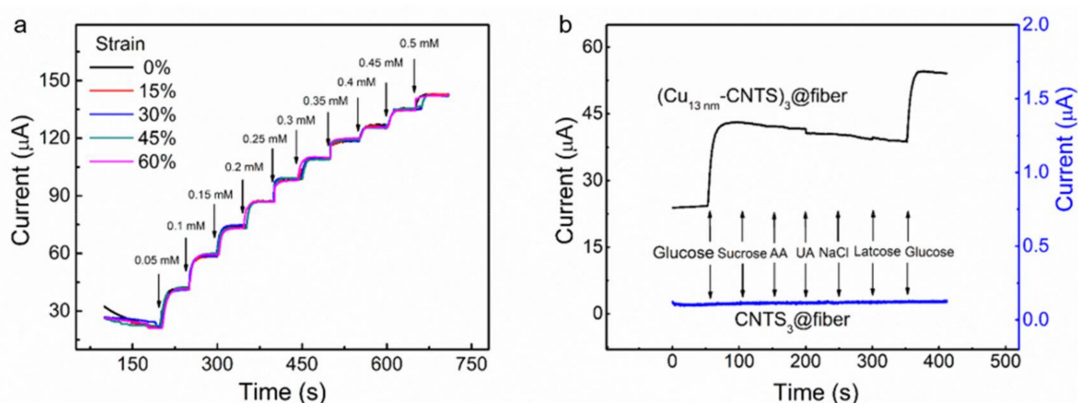


Figure 7. (a) Current as a function of time of the $(\text{Cu}_{13\text{nm}}\text{-CNTS})_3\text{@fiber}$ electrode at different strain with dropwise addition of glucose in PBS solution at 50 s interval. By adding one drop of glucose, the glucose concentration increased by 0.05 mM in the detection solution, and the detection potential was +0.35 V. (b) Current as a function of time of the $(\text{Cu}_{13\text{nm}}\text{-CNTS})_3\text{@fiber}$ electrode and $\text{CNTS}_3\text{@fiber}$ electrode with addition of glucose and interferences as indicated into PBS solution. By adding one drop of glucose, the glucose concentration increased by 0.05 mM in the detection solution, and by adding one drop of interferences, the corresponding concentration also increased as follows: sucrose (0.008 mM), AA (0.008 mM), UA (0.008 mM), NaCl solution (150 mM), and lactose (0.008 mM). The applied potential was +0.35 V.

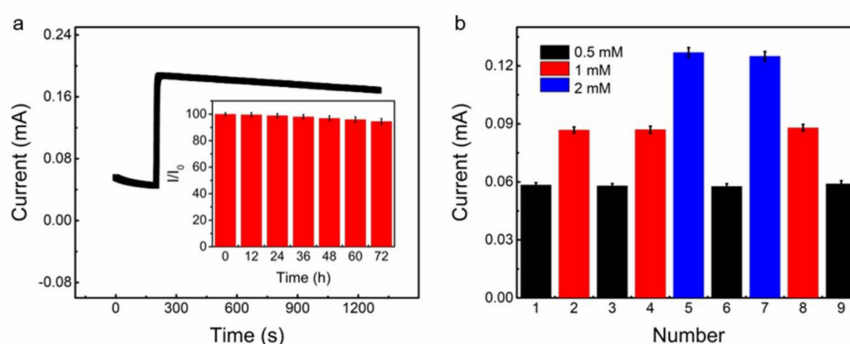


Figure 8. (a) Amperometric response of the $(\text{Cu}_{13\text{nm}}\text{-CNTS})_3$ @fiber electrode by addition of 1 mM glucose into the PBS solution and stored for a long period of running time (1000 s), The inset is the repeated measurements of the calibration curve of the relevant amperometric signal of the sensor electrode with an interval of 12 h in PBS solution during 72 h, with 1.0 mM glucose at +0.35 V. (b) The calibrated consecutive measurements of the $(\text{Cu}_{13\text{nm}}\text{-CNTS})_3$ @fiber electrode in glucose solution with different concentrations. For (a,b), nine samples (three samples from three separate batches) are used here to get the average values.

4. Conclusions

In summary, we prepared highly stretchable $(\text{Cu}_t\text{-CNTS})_m$ @fiber conductor by using buckled copper coated CNTS sheath and rubber fiber core, and demonstrated it as a non-enzymatic glucose sensing electrode. This $(\text{Cu}_t\text{-CNTS})_m$ @fiber showed a low resistance of $0.4 \Omega \cdot \text{cm}^{-1}$ at strain of 500%, and little resistance change of 27% with strain increasing from 0% to 500%. The amperometric response of the $(\text{Cu}_t\text{-CNTS})_m$ @fibers electrode for glucose detection was stable for a large strain range up to 60%, with a low detection limit of 0.05 mM, high sensitivity of $46 \text{ mA} \cdot \text{M}^{-1}$, and selectivity against sucrose, AA, lactose, UA, and high salt concentrations. The $(\text{Cu}_t\text{-CNTS})_m$ @fiber could be used as a promising candidate electrode for wearable on-body glucose monitoring.

Acknowledgments: This work was supported by the National Key Research and Development Program of China 2017YFB0307000, the National Natural Science Foundation of China (grants U1533122, 51773094, and 51508412), the Natural Science Foundation of Tianjin 16JCQNJC07000.

Author Contributions: Da-Wei Jiang, Zhong-Sheng Liu, and Zun-feng Liu conceived and designed the experiments; Kun-Kun Wu and Lin-Lin Mou performed the experiments; Raquel Ovalle-Robles, Kanzan Inoue, and Yu Zhang analyzed the data; Ning-Yi Yuan, Jian-Ning Ding, and Jian-Hua Qiu contributed materials, reagents, and analysis tools; Da-Wei Jiang and Zun-Feng Liu wrote the paper.

Conflicts of Interest: The authors declare no conflict of interest.

References

1. Wang, H.; Ma, X.H.; Hao, Y. Electronic devices for human-machine interfaces. *Adv. Mater. Interfaces* **2017**, *4*, 1600709. [[CrossRef](#)]
2. Edwards, J. Wireless sensors relay medical insight to patients and caregivers. *IEEE Signal Proc. Mag.* **2012**, *29*, 8–12. [[CrossRef](#)]
3. Haidar, Z.S. Bio-inspired/-functional colloidal core-shell polymeric-based nanosystems: Technology promise in tissue engineering, bioimaging and nanomedicine. *Polymers* **2010**, *2*, 323–352. [[CrossRef](#)]
4. Mukhopadhyay, S.C. Wearable sensors for human activity monitoring: A review. *IEEE Sens. J.* **2014**, *15*, 1321–1330. [[CrossRef](#)]
5. Wang, X.W.; Liu, Z.; Zhang, T. Flexible sensing electronics for wearable/attachable health monitoring. *Small* **2017**, *13*, 1602790. [[CrossRef](#)] [[PubMed](#)]
6. Zhu, P.; Weng, Z.Y.; Li, X.; Liu, X.M.; Wu, S.L.; Yeung, K.W.K.; Wang, X.B.; Cui, Z.D.; Yang, X.J.; Chu, P.K. Biomedical applications of functionalized ZnO nanomaterials: From biosensors to bioimaging. *Adv. Mater. Interfaces* **2016**, *3*, 1500494. [[CrossRef](#)]

7. Yamada, T.; Hayamizu, Y.; Yamamoto, Y.; Yomogida, Y.; Izadi-Najafabadi, A.; Futaba, D.N.; Hata, K. Stretchable carbon nanotube strain sensor for human motion detection. *Nat. Nanotechnol.* **2011**, *6*, 296–301. [[CrossRef](#)] [[PubMed](#)]
8. Cai, L.; Song, L.; Luan, P.; Zhang, Q.; Zhang, N.; Gao, Q.; Zhao, D.; Zhang, X.; Tu, M.; Yang, F. Super-stretchable, transparent carbon nanotube-based capacitive strain sensors for human motion detection. *Sci. Rep.* **2013**, *3*, 3402. [[CrossRef](#)]
9. Ji, T.K.; Pyo, J.; Rho, J.; Ahn, J.H.; Je, J.H.; Margaritondo, G. Three-dimensional writing of highly stretchable organic nanowires. *ACS Macro Lett.* **2012**, *1*, 375–379. [[CrossRef](#)]
10. Wang, C.; Zheng, W.; Yue, Z.; Too, C.O.; Wallace, G.G. Buckled, stretchable polypyrrole electrodes for battery applications. *Adv. Mater.* **2011**, *23*, 3580–3584. [[CrossRef](#)] [[PubMed](#)]
11. Ata, S.; Kobashi, K.; Yumura, M.; Hata, K. Mechanically durable and highly conductive elastomeric composites from long single-walled carbon nanotubes mimicking the chain structure of polymers. *Nano Lett.* **2012**, *12*, 2710–2716. [[CrossRef](#)] [[PubMed](#)]
12. Wakuda, D.; Suganuma, K. Stretchable fine fiber with high conductivity fabricated by injection forming. *Appl. Phys. Lett.* **2011**, *98*, 073304. [[CrossRef](#)]
13. Bowden, N.; Brittain, S.; Evans, A.G.; Hutchinson, J.W.; Whitesides, G.M. Spontaneous formation of ordered structures in thin films of metals supported on an elastomeric polymer. *Nature* **1998**, *393*, 146–149. [[CrossRef](#)]
14. Xu, F.; Zhu, Y. Highly conductive and stretchable silver nanowire conductors. *Adv. Mater.* **2012**, *24*, 5117–5122. [[CrossRef](#)] [[PubMed](#)]
15. Yu, C.; Masarapu, C.; Rong, J.; Wei, B.; Jiang, H. Stretchable supercapacitors based on buckled single-walled carbon-nanotube macrofilms. *Adv. Mater.* **2009**, *21*, 4793–4797. [[CrossRef](#)] [[PubMed](#)]
16. Chen, X.; Lin, H.; Chen, P.; Guan, G.; Deng, J.; Peng, H. Smart, stretchable supercapacitors. *Adv. Mater.* **2014**, *26*, 4444–4449. [[CrossRef](#)] [[PubMed](#)]
17. Chen, T.; Dai, L. Carbon nanomaterials for high-performance supercapacitors. *Mater. Today* **2013**, *16*, 272–280. [[CrossRef](#)]
18. Shang, Y.Y.; He, X.D.; Li, Y.B.; Zhang, L.H.; Li, Z.; Ji, C.Y.; Shi, E.Z.; Li, P.X.; Zhu, K.; Peng, Q.Y.; et al. Carbon Nanotubes: Super-Stretchable Spring-Like Carbon Nanotube Ropes. *Adv. Mater.* **2012**, *24*, 2935. [[CrossRef](#)]
19. Zang, J.F.; Ryu, S.; Pugno, N.; Wang, Q.M.; Tu, Q.; Buehler, M.J.; Zhao, X.H. Multifunctionality and control of the crumpling and unfolding of large-area graphene. *Nat. Mater.* **2013**, *12*, 321–325. [[CrossRef](#)] [[PubMed](#)]
20. Mu, J.; Hou, C.; Wang, G.; Wang, X.; Zhang, Q.; Li, Y.; Wang, H.; Zhu, M. An elastic transparent conductor based on hierarchically wrinkled reduced graphene oxide for artificial muscles and sensors. *Adv. Mater.* **2016**, *28*, 9491–9497. [[CrossRef](#)] [[PubMed](#)]
21. World Health Organization. *Global Report on Diabetes*; World Health Organization: Geneva, Switzerland, 2016; ISBN 978 92 4 156525 7.
22. Dawish, M.A.A.; Robert, A.A.; Braham, R.; Hayek, A.A.A.; Saeed, A.A.; Ahmed, R.A.A.; Sabaan, F.S.A. Diabetes mellitus in Saudi Arabia: A review of the recent literature. *Curr. Diabetes Rev.* **2016**, *12*, 359–368. [[CrossRef](#)] [[PubMed](#)]
23. Shi, Y.; Hu, F.B. The global implications of diabetes and cancer. *Lancet* **2014**, *383*, 1947–1948. [[CrossRef](#)]
24. Beckles, G.L.A.; Engelgau, M.M.; Narayan, K.M.V.; Herman, W.H.; Aubert, R.E.; Williamson, D.F. Population-based assessment of the level of care among adults with diabetes in the U.S. *Diabetes Care* **1998**, *21*, 1432–1438. [[CrossRef](#)] [[PubMed](#)]
25. Moyer, J.; Wilson, D.; Finkelshtein, I.; Wong, B.; Potts, R. Correlation between sweat glucose and blood glucose in subjects with diabetes. *Diabetes Technol.* **2012**, *14*, 398–402. [[CrossRef](#)] [[PubMed](#)]
26. Wang, H.Y.; Liu, Z.F.; Ding, J.N.; Lepró, X.; Fang, S.L.; Jiang, N.; Yuan, N.Y.; Wang, R.; Yin, Q.; Lv, W.; et al. Downsized sheath–core conducting fibers for weavable superelastic wires, biosensors, supercapacitors, and strain sensors. *Adv. Mater.* **2016**, *28*, 4998–5007. [[CrossRef](#)] [[PubMed](#)]
27. Zhan, B.B.; Liu, C.B.; Chen, H.P.; Shi, H.X.; Wang, L.H.; Chen, P.; Huang, W.; Dong, X.C. Free-standing electrochemical electrode based on Ni(OH)₂/3D graphene foam for nonenzymatic glucose detection. *Nanoscale* **2014**, *6*, 7424–7429. [[CrossRef](#)] [[PubMed](#)]
28. Lee, H.; Song, C.; Hong, Y.S.; Kim, M.S.; Cho, H.R.; Kang, T.; Shin, K.; Choi, S.H.; Hyeon, T.; Kim, D. Wearable/disposable sweat-based glucose monitoring device with multistage transdermal drug delivery module. *Sci. Adv.* **2017**, *3*, e1601314. [[CrossRef](#)] [[PubMed](#)]

29. Bandodkar, A.J.; Jeerapan, I.; You, J.M.; Nuñez-Flores, R.; Wang, J. Highly stretchable fully-printed CNT-based electrochemical sensors and biofuel cells: Combining intrinsic and design-induced stretchability. *Nano Lett.* **2015**, *16*, 721–727. [[CrossRef](#)] [[PubMed](#)]
30. Sappia, L.D.; Piccinini, E.; Marmisollé, W.; Santilli, N.; Maza, E.; Moya, S.; Battaglini, F.; Madrid, R.E.; Azzaroni, O. Integration of biorecognition elements on PEDOT platforms through supramolecular interactions. *Adv. Mater. Interfaces* **2017**, *4*, 1700502. [[CrossRef](#)]
31. Zubkovs, V.; Schuergers, N.; Lambert, B.; Ahunbay, E.; Boghossian, A.A. Mediatorless, reversible optical nanosensor enabled through enzymatic pocket doping. *Small* **2017**, *13*, 1701654. [[CrossRef](#)] [[PubMed](#)]
32. Oliver, N.S.; Toumazou, C.; Cass, A.E.G.; Johnston, D.G. Glucose sensors: A review of current and emerging technology. *Diabet. Med.* **2009**, *26*, 197–210. [[CrossRef](#)]
33. Li, Y.; Hodak, M.; Lu, W.; Bernholc, J. Selective sensing of ethylene and glucose using carbon-nanotube-based sensors: An ab initio investigation. *Nanoscale* **2017**, *9*, 1687–1698. [[CrossRef](#)] [[PubMed](#)]
34. Gates, B.D. Materials science: Flexible electronics. *Science* **2009**, *323*, 1566–1567. [[CrossRef](#)] [[PubMed](#)]
35. Harada, S.; Honda, W.; Arie, T.; Akita, S.; Takei, K. Fully printed, highly sensitive multifunctional artificial electronic whisker arrays integrated with strain and temperature sensors. *ACS Nano* **2014**, *8*, 3921–3927. [[CrossRef](#)] [[PubMed](#)]
36. Lee, K.; Park, J.; Lee, M.S.; Kim, J.; Hyun, B.G.; Kang, D.J.; Lee, C.Y.; Bien, F.; Park, J.U. In-situ synthesis of carbon nanotube-graphite electronic devices and their integrations onto surfaces of live plants and insects. *Nano Lett.* **2014**, *14*, 2647–2654. [[CrossRef](#)] [[PubMed](#)]
37. Yang, G.; Lee, C.; Kim, J.; Ren, F.; Pearton, S.J. Flexible graphene-based chemical sensors on paper substrates. *Phys. Chem. Chem. Phys.* **2013**, *15*, 1798–1801. [[CrossRef](#)] [[PubMed](#)]
38. Zhu, G.; Yang, W.Q.; Zhang, T.; Jing, Q.; Chen, J.; Zhou, Y.S.; Bai, P.; Wang, Z.L. Self-powered, ultrasensitive, flexible tactile sensors based on contact electrification. *Nano Lett.* **2014**, *14*, 3208–3213. [[CrossRef](#)] [[PubMed](#)]
39. Elouarzaki, K.; Bourourou, M.; Holzinger, M.; Goff, A.L.; Marks, R.S.; Cosnier, S. Freestanding HRP–GOx redox buckypaper as an oxygen-reducing biocathode for biofuel cell applications. *Energy Environ. Sci.* **2015**, *8*, 2069–2074. [[CrossRef](#)]
40. Zang, Y.; Zhang, F.; Di, C.; Zhu, D. Advances of flexible pressure sensors toward artificial intelligence and health care applications. *Mater. Horiz.* **2015**, *2*, 140–156. [[CrossRef](#)]
41. He, W.; Sun, Y.; Xi, J.; Abdurhman, A.A.; Ren, J.; Duan, H. Printing graphene-carbon nanotube-ionic liquid gel on graphene paper: Towards flexible electrodes with efficient loading of PtAu alloy nanoparticles for electrochemical sensing of blood glucose. *Anal. Chim. Acta* **2015**, *903*, 61–68. [[CrossRef](#)] [[PubMed](#)]
42. Tian, K.; Prestgard, M.; Tiwari, A. A review of recent advances in nonenzymatic glucose sensors. *Mater. Sci. Eng. C Mater.* **2014**, *41*, 100–118. [[CrossRef](#)] [[PubMed](#)]
43. Kung, C.W.; Cheng, Y.H.; Ho, K.C. Single layer of nickel hydroxide nanoparticles covered on a porous Ni foam and its application for highly sensitive non-enzymatic glucose sensor. *Sens. Actuators B Chem.* **2014**, *204*, 159–166. [[CrossRef](#)]
44. Iwu, K.O.; Lombardo, A.; Sanza, R.; Scirè, S.; Mirabella, S. Facile synthesis of Ni nanofoam for flexible and low-cost non-enzymatic glucose sensing. *Sens. Actuators B Chem.* **2015**, *224*, 764–771. [[CrossRef](#)]
45. Soomro, R.A.; Ibupoto, Z.H.; Sirajuddina; Abro, M.I.; Willander, M. Electrochemical sensing of glucose based on novel hedgehog-like NiO nanostructures. *Sens. Actuators B Chem.* **2015**, *209*, 966–974. [[CrossRef](#)]
46. Guo, C.Y.; Wang, Y.M.; Zhao, Y.Q.; Xu, C.L. Non-enzymatic glucose sensor based on three dimensional nickel oxide for enhanced sensitivity. *Anal. Methods* **2013**, *5*, 1644–1647. [[CrossRef](#)]
47. Ibupoto, Z.H.; Khun, K.; Beni, V.; Liu, X.J.; Willander, M. Synthesis of novel CuO nanosheets and their non-enzymatic glucose sensing applications. *Sensors* **2013**, *13*, 7926–7938. [[CrossRef](#)] [[PubMed](#)]
48. Li, H.M.; Wang, J.H.; Wang, Q.G.; Qian, X.; Qian, Y.; Yang, M.; Li, F.Y.; Lu, H.; Wang, H. Chemical fractionation of arsenic and heavy metals in fine particle matter and its implications for risk assessment: A case study in Nanjing, China. *Atmos. Environ.* **2015**, *103*, 339–346. [[CrossRef](#)]
49. Li, M.; Bo, X.J.; Zhang, Y.F.; Han, C.; Guo, L.P. One-pot ionic liquid-assisted synthesis of highly dispersed PtPd nanoparticles/reduced graphene oxide composites for nonenzymatic glucose detection. *Biosens. Bioelectron.* **2014**, *56*, 223–230. [[CrossRef](#)] [[PubMed](#)]
50. Huang, J.F.; Zhu, Y.H.; Chen, W.; Zhou, Y.; Li, C.Z. Flexible 3D porous CuO nanowire arrays for enzymeless glucose sensing: In situ engineered versus ex situ piled. *Nanoscale* **2015**, *7*, 559–569. [[CrossRef](#)] [[PubMed](#)]

51. Xiao, F.; Li, Y.Q.; Gao, H.C.; Ge, S.B.; Duan, H.W. Growth of coral-like PtAu–MnO₂ binary nanocomposites on free-standing graphene paper for flexible nonenzymatic glucose sensors. *Biosens. Bioelectron.* **2013**, *41*, 417–423. [[CrossRef](#)] [[PubMed](#)]
52. Kim, W.S.; Lee, G.J.; Ryu, J.H.; Park, K.C.; Park, H.K. A flexible, nonenzymatic glucose biosensor based on Ni-coordinated, vertically aligned carbon nanotube arrays. *RSC Adv.* **2014**, *4*, 48310–48316. [[CrossRef](#)]
53. Ruan, J.L.; Chen, C.; Shen, J.H.; Zhao, X.L.; Qian, S.H.; Zhu, Z.G. A gelated colloidal crystal attached lens for noninvasive continuous monitoring of tear glucose. *Polymers* **2017**, *9*, 125. [[CrossRef](#)]
54. Lee, J.; Ko, S.; Kwon, C.H.; Lima, M.D.; Baughman, R.H.; Kim, S.J. Artificial muscle: Carbon nanotube yarn-based glucose sensing artificial muscle. *Small* **2016**, *12*, 2100. [[CrossRef](#)]
55. Liu, Z.F.; Fang, S.L.; Moura, F.A.; Ding, J.N.; Jiang, N.; Di, J.T.; Zhang, M.; Lepró, X.; Galvão, D.S.; Haines, C.S.; et al. Hierarchically buckled sheath-core fibers for superelastic electronics, sensors, and muscles. *Science* **2015**, *349*, 400–404. [[CrossRef](#)] [[PubMed](#)]
56. Yi, W.; Liu, J.; Chen, H.B.; Li, H.M. Copper/nickel nanoparticle decorated carbon nanotubes for nonenzymatic glucose biosensor. *J. Solid State Electron.* **2015**, *19*, 1511–1521. [[CrossRef](#)]
57. Qin, X.Y.; Lu, W.B.; Luo, Y.L.; Chang, G.H.; Asiri, A.M.; Al-Youbi, A.; Sun, X.P. Synthesis of Ag nanoparticle-decorated 2,4,6-tris(2-pyridyl)-1,3,5-triazine nanobelts and their application for H₂O₂ and glucose detection. *Analyst* **2012**, *137*, 939–943. [[CrossRef](#)] [[PubMed](#)]
58. Luo, J.; Jiang, S.S.; Zhang, H.Y.; Jiang, J.; Liu, X.Y. A novel non-enzymatic glucose sensor based on Cu nanoparticle modified graphene sheets electrode. *Anal. Chim. Acta* **2012**, *709*, 47–53. [[CrossRef](#)] [[PubMed](#)]
59. Tong, S.F.; Xu, Y.H.; Zhang, Z.X.; Song, W.B. Dendritic bimetallic nanostructures supported on self-assembled titanate films for sensor application. *J. Phys. Chem. C* **2010**, *114*, 20925–20931. [[CrossRef](#)]
60. Lv, W.; Jiang, N.; Ding, J.N.; Liu, Z.F.; Yuan, N.Y.; Ovalle-Robles, R.; Inoue, K.; Lepró, X.; Zhang, M. Three-dimensional conducting elastomeric composites based on buckling carbon nanotube sheets for interconnects and temperature sensor. *J. Nanosci. Nanotechnol.* **2017**, *17*, 1934–1941. [[CrossRef](#)]
61. Zhang, M.; Fang, S.L.; Zakhidov, A.; Lee, S.B.; Aliev, A.E.; Williams, C.D.; Atkinson, K.R.; Baughman, R.H. Strong, transparent, multifunctional, carbon nanotube sheets. *Science* **2005**, *309*, 1215–1219. [[CrossRef](#)] [[PubMed](#)]
62. Arvinte, A.; Sesay, A.M.; Virtanen, V. Carbohydrates electrocatalytic oxidation using CNT–NiCo-oxide modified electrodes. *Talanta* **2011**, *84*, 180–186. [[CrossRef](#)] [[PubMed](#)]
63. Wang, R.; Jiang, N.; Su, J.; Yin, Q.; Zhang, Y.; Liu, Z.S.; Lin, H.B.; Moura, F.A.; Yuan, N.Y.; Roth, S.; et al. A Bi-sheath fiber sensor for giant tensile and torsional displacements. *Adv. Funct. Mater.* **2017**, *27*, 1702134. [[CrossRef](#)]
64. Pierson, J.; Wiederkehr, D.; Billard, A. Reactive magnetron sputtering of copper, silver, and gold. *Thin Solid Films* **2005**, *478*, 196–205. [[CrossRef](#)]
65. Li, S.; Su, Y.W.; Li, R. Splitting of the neutral mechanical plane depends on the length of the multi-layer structure of flexible electronics. *Proc. R. Soc. Lond. A* **2016**, *472*, 20160087. [[CrossRef](#)] [[PubMed](#)]
66. Lacour, S.; Wagner, S.; Huang, Z.Y.; Suo, Z.G. Stretchable gold conductors on elastomeric substrates. *Appl. Phys. Lett.* **2003**, *82*, 2404–2406. [[CrossRef](#)]
67. Efimenko, K.; Rackaitis, M.; Manias, E.; Vaziri, A.; Mahadevan, L.; Genzer, J. Nested self-similar wrinkling patterns in skins. *Nat. Mater.* **2005**, *4*, 293–297. [[CrossRef](#)] [[PubMed](#)]

